BEHAVIOR OF FRP-CONFINED NORMAL- AND HIGH-STRENGTH CONCRETE UNDER CYCLIC AXIAL COMPRESSION

Togay Ozbakkaloglu[1] and Emre Akin[2]

ABSTRACT

An important application of fiber reinforced polymer (FRP) composites is as a confining material for concrete, in both the seismic retrofit of existing reinforced concrete columns and in the construction of concrete-filled FRP tubes as earthquake-resistant columns in new construction. The reliable design of these structural members against earthquake-induced forces necessitates a clear understanding of the stress-strain behavior of FRP-confined concrete under load cycles. This paper presents the results of an experimental study on the behavior of FRP-confined normal- and high-strength concrete under axial compression. A total of 24 aramid and carbon FRP-confined concrete cylinders with different concrete strengths and FRP jacket thicknesses were tested under monotonic and cyclic loading. Examination of the test results have lead to a number of significant conclusions in regards to both the trend and ultimate condition of the axial stress-strain behavior of FRP-confined concrete. These results are presented and a discussion is provided on the influence of the main test parameters in the observed behaviors. The results are also compared with two existing cyclic axial stress-strain models for FRP-confined concrete.

KEYWORDS: Fiber reinforced polymers; Concrete; High-strength concrete; Confinement; Cyclic loading; Stress-strain behavior.

[1] (Corresponding author) Senior Lecturer, School of Civil, Environmental and Engineering, University of Adelaide, Australia. Tel : + 618 8303 6477; Fax : +618 8303 4359; Email: tozbakka@civeng.adelaide.edu.au
[2] Research Fellow, Department of Civil Engineering, Selcuk University, Konya, Turkey.

INTRODUCTION

Owing to their favorable material properties, fiber reinforced polymer (FRP) composites have become increasingly popular in the construction industry over the last two decades. An important application of FRP composites is as a confining material for concrete, in both the seismic retrofit of existing reinforced concrete columns and in the construction of concrete-filled FRP tubes as earthquake-resistant columns in new construction. For the safe and reliable design of these structural members, it is necessary to properly understand and model the stress-strain behavior of FRP-confined concrete. Of particular importance is the understanding of the behavior of FRP-confined concrete under cyclic axial compression for the seismic retrofit and design of these members.

The monotonic axial stress-strain behavior of FRP-confined concrete has been studied extensively over the past two decades, which have lead to the development of over 70 stress-strain models (e.g., Samaan et al. 1998; Xiao and Wu 2000; Fam and Rizkalla 2001; Lam and Teng 2003; Binici 2005; Jiang and Teng 2006; Fahmy and Wu 2010; Xiao et al. 2010). In contrast, only a few studies have so far investigated the behavior of FRP-confined concrete under cyclic axial compression (Mirmiran and Shahawy 1997; Rodrigues and Silva 2001; Rousakis 2001; Ilki and Kumbasar 2003; Shao et al. 2006; Lam et al. 2006; Lam and Teng 2009; Abbasnia and Ziaadiny 2010) and, to the best knowledge of the authors, only two analytical cyclic stress-strain models (Shao et al. 2006, Lam and Teng 2009) have been proposed in the open literature. While these studies have provided valuable insights into certain aspects of the problem, there are a number of other important aspects, such as the influence of the concrete strength and type of FRP, that are yet to be explored.

Not unlike that of FRP, the popularity of high-strength concrete (HSC) in the construction industry has been on a steady incline during the last two decades. It is now understood that HSC offers superior performance and economy over normal-strength concrete (NSC) when used in the

construction of bridges and multi-story buildings. However, HSC structural members are known to exhibit brittle behavior, which jeopardizes their use in seismically active regions. Yet, it is well established that lateral confinement of concrete can greatly enhance its ductility; though, it is also established that HSC require more confinement than NSC because the confinement demand of concrete increases proportionally with its strength. Indeed, experimental studies conducted by Ozbakkaloglu and Saatcioglu (2006, 2007) on the seismic behavior of FRP-confined HSC columns demonstrated that the lateral deformation capacity of HSC columns can be substantially increased by the use of FRP tubes as concrete confinement. The majority of the existing studies on the axial compressive behavior of FRP-confined concrete have focused on NSC with strengths less than 55 MPa, and only a few studies have been concerned with FRP-confined HSC (Berthet et al. 2005; Mandal et al. 2005; Almusallam 2007; Eid et al 2009; Vincent and Ozbakkaloglu 2009; Wu et al. 2009; Cui and Sheikh 2010; Xiao et al. 2010). As has also been recently reported by Xiao et al. (2010), existing test results are insufficient for clear understanding of the axial compressive behavior of FRP-confined HSC. Likewise, a review of the existing literature indicates that the majority of the existing studies on the axial compressive behavior of FRP-confined concrete have focused on carbon and glass FRP (CFRP and GFRP) confined concrete, with the behavior of concretes confined by other composite materials, such as aramid FRP (AFRP) or high-modulus CFRP (HM CFRP), receiving relatively limited attention.

This paper presents the results of an experimental study which was aimed at filling the existing research gaps outlined above. The experimental program focused on the behavior of CFRP-confined HSC and AFRP-confined NSC and HSC under monotonic and cyclic axial compression, and it was the first comprehensive study reported in the literature on the axial cyclic behavior of FRP-confined HSC. The results of the experimental program are first presented, followed by a discussion on the influence of the main test parameters on the test results. These results are then compared with two cyclic axial stress-strain models proposed for FRP-confined concrete.

EXPERIMENTAL PROGRAM

Test Specimens and Materials

A total of 24 FRP-confined concrete cylinders with a concrete core diameter of 152.5 mm and a height of 305 mm were manufactured and tested under axial compression. The test parameters included the concrete compressive strength (i.e., NSC and HSC), type of FRP material (i.e., CFRP and AFRP), FRP thickness (i.e., 2 to 6 layers), and loading pattern (i.e., axial monotonic and axial cyclic).

The specimens were prepared using NSC and HSC mixes, with average unconfined concrete compressive strengths 39 MPa and 103 MPa attained during the period of testing. Both mixes consisted of crushed bluestone as the coarse aggregate with a nominal maximum size of 10 mm. Silica fume was added to the HSC mix at 8 percent of the binder content by weight. The NSC specimens were cast of a single batch, whereas two separate batches were prepared for the HSC specimens. The testing of the HSC specimens started right after the attainment of the 28-day strength and continued for approximately 3 weeks. Concrete cylinder tests have been conducted through the testing program to accurately record the variations in the strength of unconfined concrete during testing. The unconfined concrete strengths f'_{co} at the day of testing are reported together with the corresponding axial strains ε_{co} in Table 1 for each specimen. ε_{co} values were not measured directly for all the control specimens but were calculated using the expression given by Tasdemir (1998).

The specimens were confined by either CFRP or AFRP jackets. AFRP was used for the confinement of both NSC and HSC, whereas CFRP was used only for the jacketing of HSC specimens. In determining the number of FRP layers of the specimens, due consideration was given to the well-understood influence of the concrete strength on the confinement demand (Martinez et al. 1984; Yong et al. 1988; Razvi and Saatcioglu 1994). The FRP jackets of the 22 of the specimens

were formed by manually wrapping impregnated FRP sheets around the concrete cylinders in the hoop direction. Two of the specimens (i.e., H-C-4L-M1 and H-C-6L-M2) were confined by formerly manufactured CFRP tubes instead of wrapping. Similar to the wrapped specimens, these tubes were prepared using a manual wet lay-up process by wrapping epoxy resin impregnated fiber sheets around precision-cut high-density Styrofoam templates in the hoop direction. An overlap length of 100 mm was provided in all specimens to prevent premature debonding failure. Specimens confined with 2 and 3 layers of FRP were wrapped with a single FRP sheet continuously, whereas specimens confined with 4 and 6 layers of FRP were wrapped by two FRP sheets, and hence had two overlap regions. The details of the test specimens are given in Table 1 and the properties of the unidirectional carbon and aramid fiber sheets used in the manufacturing of the FRP jackets are provided in Table 2. Two nominally identical specimens were tested for each unique specimen/loading configuration.

Specimen Designation

The specimens in Tables 1 and 3 were labeled as follows: letters N and H were used to label "NSC" and “HSC”. This was followed by a letter "A" or "C", which were used in labeling “aramid” and “carbon” FRP. The number of FRP layers was given next, and was followed by a letter M for "monotonic" or C for "cyclic" loading. The final numbers 1 or 2 were used to make distinction between two nominally identical specimens. For instance, N-A-2L-C1 is the first of the two identical specimens that were made of NSC confined with 2-layers of AFRP, and tested under cyclic loading.

Test Setup and Instrumentation

Axial deformations of the specimens were measured with four linear variable displacement transducers (LVDTs), which were mounted at the corners between the loading and supporting steel plates of the test machine as shown in Fig. 1. The recorded deformations were used in the calculation of the average axial strains along the height of the specimens. In addition, the specimens

were also instrumented at the mid-height with two unidirectional strain gauges with a gauge length of 20 mm to measure axial strains. These strain gauge readings were used to correct the LVDT measurements at the early stages of loading, where additional displacements due to closure of the gaps in the setup were also recorded by the LVDTs. Transverse strains were measured by three unidirectional strain gauges having a gauge length of 20 mm that were bonded on the FRP jacket outside the overlap region.

The specimens were tested under axial compression using a 5000 kN capacity universal testing machine. Initial elastic portion of monotonic and cyclic loading and unloading/reloading cycles of the cyclic loading were performed with load control at 3 kN per second, whereas displacement control was used at approximately 0.01 mm per second for the entire response of monotonically loaded specimens beyond initial softening, and for the segments between each unloading curve for cyclically loaded specimens. Prior to testing, all specimens were capped at both ends with a thin layer of high-strength capping material to ensure uniform distribution of the applied pressure, and the load was applied directly to the concrete core thorough the use of two precision-cut high-strength steel discs with 150 mm diameter and 15 mm thickness, as illustrated in Fig.1. For 12 of the specimens, loading was increased monotonically until failure. For the remaining twelve specimens, cyclic compression involving unloading and reloading cycles was applied at approximately 0.15% axial strain intervals. These specimens were subjected to a single unloading/reloading cycle at each prescribed axial strain level. A small axial load of 30 kN was maintained during the unloading/reloading cycles to prevent any undesired movement in the specimen. Test setup and instrumentation are shown in Fig. 1.

TEST RESULTS

Failure mode

Typical failures of the test specimens are shown in Fig. 2. All of the specimens failed by rupture of the FRP jacket. As can be seen in Fig. 2, two different types of damage were observed in the concrete depending on its compressive strength. Concrete shear cones were formed in the NSC specimens, as illustrated in Fig. 2(a), suggesting gradual concrete crushing took place in these specimens. On the other hand, in the HSC specimens the damage was highly localized around a major shear crack, as shown in Fig. 2(b).

Axial stress-strain behavior

The summary of the key experimental results are shown in Table 3, which include: the FRP hoop rupture strains ($\varepsilon_{h,rup.}$), ultimate axial strength and strain of confined concrete (f'_{cc} *and* ε_{cu}), and strength and strain enhancement ratios (f'_{cc} /f'_{co} *and* ε_{cu}/ ε_{co}). The ultimate confined-concrete strengths f'_{cc} were calculated from the recorded axial loads just prior to the failure of the specimens. The ultimate axial strain of confined concrete ε_{cu} was averaged from the four LVDTs, and the hoop rupture strains $\varepsilon_{h,rupt}$ were averaged from three strain gauge readings, unless stated otherwise in Table 3. The key specimen performance indicators, namely the strength enhancement coefficient k_1, strain enhancement coefficient k_2, and strain reduction factor k_ε are also given in Table 3. These indicators are discussed in detail later in the paper.

Axial stress-strain curves of the cyclically tested specimens of the present study are shown in Fig. 3. In each of the charts shown in Fig. 3, stress-strain curves of two nominally identical monotonically loaded specimens are also included for comparison. Figure 3 illustrates that the stress-strain curves of monotonically loaded specimens exhibit an ascending first branch that is followed by an ascending or an almost flat second branch. As expected, the stress-strain behavior in the second branch is influenced significantly by the important confinement parameters, including the unconfined concrete strength and type and amount of confining material. It can be observed in Fig. 3 that most of the HSC specimens experienced a sudden drop in strength starting right at the

transition point on the stress-strain curve. This phenomenon, which can be referred to as 'initial strength softening', can be associated to the brittle nature of the higher strength concretes. During this stage, the hoop strains recorded on the FRP jacket increased rapidly and at one point confining pressures generated by the FRP jacket reached to a level that was high enough to sufficiently confine the HSC. This point corresponds to the plateau formation on the stress-strain curves shown in Fig.3, which follows the initial strength softening region. Further increase in the axial strains leads to either an almost flat or a slightly ascending type of final portion in the stress-strain curve of FRP-confined HSC specimens as illustrated in Fig. 3. The stress-strain curves of NSC specimens, on the other hand, are of a continuously ascending type with no signs of softening throughout the response history, as can be seen in Fig. 3.

Table 3 shows that the majority of the cyclically loaded specimens exhibit higher compressive strengths and ultimate axial strains than their monotonically loaded counterparts. A similar phenomenon was previously reported by other researchers for FRP-confined NSC (Rousakis 2001; Lam et al. 2006), who demonstrated that load cycles resulted in increased hoop rupture strains leading to increased compressive strength and ultimate axial strain. These effects are discussed further in the following sections of the paper. The comparison of the behaviors of otherwise identical tube encased and wrapped specimens (i.e., H-C-4L-M and H-C-6L-M series specimens) in Fig. 3 reveals no significant difference between the axial stress-strain behaviors of these specimens. Therefore, no further consideration is given to the differences of these specimens in the following discussions.

DISCUSSIONS

The envelope curve

The envelope curve of concrete represents the upper boundary of the response of the concrete under cyclic axial compression. According to the hypothesis proposed by Karsan and Jirsa (1969), a unique envelope curve exists for a given cyclically loaded concrete specimen and it is identical to

the stress-strain curve of the same concrete under monotonic loading. This hypothesis was then verified by subsequent studies on unconfined and steel-confined concrete, and was shown by Lam et al. (2006) and Abbasnia and Ziaadiny (2010) to be also valid for FRP-confined concrete.

To allow comparisons of the stress-strain curves of monotonically and cyclically tested specimens, Fig. 3 also shows the envelope curves, which were drawn by connecting the initial unloading points on the stress-strain curves of cyclically loaded specimens. Figure 3 illustrates that the envelope stress-strain curves of cyclically loaded specimens closely follow the stress-strain curves of the corresponding monotonically loaded specimens. This observation is consistent with that reported in Lam et al. (2006), and supports their conclusion that the basic hypothesis of envelope curves is valid for FRP-confined concrete.

Unloading and reloading paths and the plastic strain

To define the complete axial stress-strain response of a cyclically loaded specimen, in addition to the envelope curve, unloading and reloading paths are also required. An unloading path is defined as the stress-strain path traced by the concrete as its axial strain reduces, and a reloading path is defined as the stress-strain path traced by concrete as its axial strain increases from a starting point on an unloading path (Lam and Teng 2009). Unloading may be from a point on the envelope curve or from a point on a reloading curve (i.e., before reaching the envelope curve on the reloading path). All of the cyclically tested specimens of the present study were unloaded from their envelope curves; thus, herein the term 'unloading' refers to 'envelope curve unloading'. The axial strain at the starting point of unloading path is referred to as the envelope unloading strain $\varepsilon_{un,env}$.

An unloading path intersects the axial strain axis at a strain value that is referred to as the residual plastic strain ε_{pl}. The residual plastic strain of concrete can be defined as the residual axial strain of the material when it is unloaded to the zero stress (Lam et al. 2006). Accurate determination of the

plastic strains is of vital importance for the overall performance of cyclic axial stress-strain models. The relationship between $\varepsilon_{un,env}$ and ε_{pl} forms an important aspect of cyclic behavior and has been investigated in a number of studies for unconfined, steel-confined and FRP-confined concrete (e.g., Bahn and Hsu 1998; Sakai, J. and Kawashima 2006; Lam et al 2006; Abbasnia and Ziaadiny 2010). Lam et al. (2006) demonstrated that the relationship between unloading strains $\varepsilon_{un,env}$ and plastic strains ε_{pl} was linear for CFRP-confined NSC cylinders for $\varepsilon_{un,env} \geq 0.0035$. This observation was then supported by that of Abbasnia and Ziaadiny (2010), which was based on an experimental investigation on CFRP-confined NSC square prisms.

The relationships between the envelope unloading strains $\varepsilon_{un,env}$ and estimated plastic strains ε_{pl} are shown in Fig. 4 separately for AFRP-confined NSC, AFRP-confined HSC and CFRP-confined HSC specimens of the present study. As discussed previously, unloading curves of all the specimens were terminated just before reaching to zero stress, so the plastic strains were estimated by extending the unloading curves to cross the axial strain axis. It should also be noted that the trend lines shown in Fig. 4 are given for the unloading strains that are greater than or equal to 0.0035.

A number of important observations can be made from the examination of the trend lines shown in Figure 4. Firstly, as illustrated in each of the charts shown in Fig. 4, the trend lines of the specimens of the same concrete strength and confinement material almost coincide, which suggests that the amount of confinement has little or no influence on the residual plastic strain of FRP-confined concrete. This observation is in agreement with that previously reported by Lam et al. (2006) on CFRP-confined NSC, and it suggests that Lam et al.'s original observation is equally applicable to FRP-confined HSC and concretes confined with different types of FRP (i.e. AFRP and CFRP). Another important observation is that the comparison of the trend lines of AFRP-confined and CFRP-confined HSC specimens in Figs. 4(b) and 4(c) indicate that the trend line equation is

influenced only slightly by the type of FRP material. Finally, the comparison of the trend line equations of NSC and HSC specimens in Fig. 4 indicate that the trend line equation does not change significantly with the unconfined concrete strength. This important observation is not in agreement with the expression given in Lam and Teng's model (2009) (Eq.1), which predicts a reduction in plastic strain ε_{pl} with increasing unconfined concrete strength. Eq.1 was calibrated for HSC primarily on the extremely limited experimental data reported by Rousakis (2001) on CFRP-confined HSC. As illustrated in Fig.5, which shows the comparison of the experimental plastic strains with the predictions by Eq.1, the plastic strains of the HSC specimens of the present study are largely underestimated by Lam and Teng's model. This is discussed further under 'Comparison with existing stress-strain models'.

$$\varepsilon_{pl} = (0.87 - 0.004 f'_{co})\varepsilon_{un,env} - 0.0016 \qquad \text{for} \qquad \varepsilon_{un,env} \geq 0.0035 \qquad (1)$$

To summarize, according to the trend line expressions given in Fig. 4, none of the three important specimen parameters investigated in the present study (i.e., the concrete strength, type of FRP, and amount of confinement) appear to have significant influence on the relationship between the unloading strain $\varepsilon_{un,env}$ and residual plastic strain ε_{pl} of FRP-confined concrete. Another important specimen parameter, the shape of the specimen cross-section, has recently been reported by Abbasnia and Ziaadiny (2010) to also have only minor influence on the plastic strains of FRP-confined concrete. This conclusion was based on the comparison of the trend line equation Abbasnia and Ziaadiny (2010) obtained from their CFRP-confined NSC prismatic specimen tests with the ones reported by Lam et al. (2006) based on CFRP-confined NSC cylinder tests. It is worth noting that the relationships observed between the unloading strains $\varepsilon_{un,env}$ and plastic strains ε_{pl} in the present study are in fairly close agreement with those observed in the two aforementioned experimental studies, namely Lam et al. (2006) (Eq.2) and Abbasnia and Ziaadiny (2010) (Eq.3).

$$\varepsilon_{pl} = \begin{cases} 0.703\varepsilon_{un,env} - 0.0014 & (\textit{Series I} - \text{1-}\textit{ply CFRP}) \\ 0.716\varepsilon_{un,env} - 0.0016 & (\textit{Series II} - \text{2-}\textit{ply CFRP}) \end{cases} \qquad \text{for} \qquad \varepsilon_{un,env} \geq 0.0035 \qquad (2)$$

$$\varepsilon_{pl} = 0.747\varepsilon_{un,env} - 0.001 \qquad \text{for} \qquad \varepsilon_{un,env} > 0.0035 \qquad (3)$$

In the existing literature, in addition to the studies cited above, the model proposed by Shao et al. (2006) also provides a set of equations for the calculation of the plastic strains. However, in this model the relationship between the unloading strains and residual plastic strains is not specified explicitly, and plastic strains ε_{pl} are calculated by Eq.4 through the use of secant slopes of the unloading curves, which was defined by the originators of the model as the secant modulus of the unloading branch (E_{secu}) (Eq.5).

$$\varepsilon_{pl} = \varepsilon_{un,env} - \frac{\sigma_{un,env}}{E_{\sec u}} \qquad (4)$$

$$\frac{E_{\sec u}}{E_c} = \begin{cases} 1, & 0 \le \sigma_{un,env} / f'_{co} < 1 \\ -0.44\sigma_{un,env} / f'_{co} + 1.44, & 1 \le \sigma_{un,env} / f'_{co} < 2.5 \\ 0.34, & \sigma_{un,env} / f'_{co} \ge 2.5 \end{cases} \qquad (5)$$

where $\sigma_{un,env}$ is the stress at the envelope unloading strain, and the elastic modulus of unconfined concrete was defined as $E_c = 3950\sqrt{f'_{co}}$ (MPa), as originally proposed by Samaan et al. (1998).

The comparison of the experimental plastic strains obtained in the present study with the predictions by Eqs. 4 and 5 from model of Shao et al. (2006) is shown in Fig. 6. The figure illustrates that the plastic strain of the specimens of the present study is overestimated by Shao's model. This shortcoming of the model was originally reported by Lam et al. (2006), and it is caused by the overestimation of the unloading modulus E_{secu} by Eq.5. At any stage of the loading history beyond the initial elastic portion, with increasing deformations the unloading stiffnesses of both the NSC and HSC specimens of the present study softened much more significantly than that predicted by Eq.5. Furthermore, in Eq.5, E_{secu} is defined as a function of $\sigma_{un,env} / f'_{co}$ ratio, according to which E_{secu} decreases with an increase in $\sigma_{un,env} / f'_{co}$ ratio. This implies that, for a given unloading strain $\varepsilon_{un,env}$, unloading modulus of more heavily confined specimens with steep ascending second

branches would be lower than those of their more lightly counterparts. This is not supported by the observations from the comparison of the unloading curves of neither the NSC (i.e., N-A-2L and N-A-3L series) nor the HSC (i.e., H-A-4L and H-A-6L) specimens of the present study. In fact, the results indicate that, for a given $\varepsilon_{un,env}$ or $\sigma_{un,env}$, the unloading stiffnesses of the well-confined specimens were consistently higher than those of their more lightly confined counterparts. On the other hand, the final unloading stiffnesses of the NSC specimens of the present study agree well with the multiplier 0.34 recommended in Eq.5, which suggests an approximately two-thirds reduction in the initial elastic modulus (E_c). However, the slopes of the final unloading curves of the HSC specimens were significantly steeper, with an E_{secu}/E_c ratio of approximately 0.65 for the final unloading cycle, suggesting a much lower degree of stiffness softening. Within the confinement range considered in the present study, E_{secu}/E_c ratio is not influenced significantly by the amount of confinement for neither the HSC nor the NSC specimens. Furthermore, the comparison of the AFRP- and CFRP-confined HSC specimens indicates that the type of FRP also has a negligible influence on the final unloading stiffness.

Although, as discussed above, Shao's model consistently overestimated the plastic strains of the specimens of the present, a closer inspection of Fig. 6(a) reveals that for the NSC specimens confined with 3 layers of AFRP, model predictions of the plastic strains start to become more accurate at larger axial strain levels. For example, in the last few load cycles of both N-A-3L series specimens, Shao's model closely predicts the experimental plastic strains. This is due to the way the unloading modulus E_{secu} is defined in Eq.5 as a function of $\sigma_{un,env} / f'_{co}$ ratio. That is, Shao's model suggests a reduction in the unloading modulus with an increase in the $\sigma_{un,env} / f'_{co}$ ratio, which in turn reduces the plastic strain calculated by Eq.3 thereby making them more consistent with experimentally observed values. Because the strength enhancement due to confinement was not as pronounced in the other specimens of the present study compared to that experienced by N-A-3L series specimens, such convergence is not observed in the remaining specimens, as evident in Fig.

6. The observations and discussion presented herein suggest that the variation of the stiffness of the unloading curve can be predicted more accurately through an expression that makes use of unloading strain to ultimate axial strain ratios ($\varepsilon_{un,env}$ / ε_{cu}) while giving due consideration to the influence of the unconfined concrete strength on the stiffness softening of the unloading curve. It is clear that further research on the axial cyclic behavior of FRP-confined concrete is required to establish these key relationships.

Ultimate Condition

The ultimate condition of FRP-confined concrete is often characterized as the ultimate strength and axial strain of concrete recorded at the rupture of the FRP jacket. This, together with the fact that FRP-confined concrete often exhibits an ascending type of second branch, makes the relationship between the ultimate strength f'_{cc}, ultimate axial strain ε_{cu} and hoop rupture strain $\varepsilon_{h,rup}$ an intimate one. To better understand this relationship, FRP hoop rupture strains recorded on each test specimen are reported in Table 3 together with f'_{cc} and ε_{cu}.

The influence of the key test parameters on the ultimate condition of FRP-confined concrete that were identified in the preceding section are discussed herein. In order to make a rational assessment of the influences of unconfined concrete strength and type of FRP, the comparisons were made between the specimens having similar levels of confinement. Nominal ultimate confinement ratios f_{lu}/f'_{co}, which are reported in Table 3 and calculated from Eq.6 assuming a uniform confinement distribution, were used to establish relative confinement levels of the specimens.

$$\frac{f_{lu}}{f'_{co}} = \frac{2E_f t_f \varepsilon_{fu}}{Df'_{co}} \quad (6)$$

where E_f is the modulus of elasticity, t_f is the total nominal thickness and ε_{fu} is the ultimate tensile strain of the fibers and D is the diameter of the specimen.

It is now well understood, however, that f_{lu} / f'_{co} ratio calculated from Eq.6 is of theoretical value and it does not accurately represent the actual confining pressures developed in the FRP jacket at ultimate. As was discussed in a number of studies previously (e.g., Pessiki et al. 2001; Lam and Teng 2004; Ozbakkaloglu and Oehlers 2008), this is due to the fact that the ultimate hoop strain $\varepsilon_{h,rup}$ reached in the FRP jacket is often smaller than the ultimate tensile strain of the fibers ε_{fu}, which necessitates the use of a strain reduction factor k_ε in the calculation of the actual confining pressures at ultimate $f_{lu,a}$

$$k_\varepsilon = \frac{\varepsilon_{h,rup}}{\varepsilon_{fu}} \tag{7}$$

$$f_{lu,a} = \frac{2E_f t_f \varepsilon_{h,rup}}{D} \tag{8}$$

Table 3 gives the average strain reduction factors k_ε for the specimens of the present study in six sub-groups, which were formed based on the concrete strength and FRP type of the specimens, and the loading patterns used in testing them. It should be noted that the most damaged sections of the specimens not always corresponded to the sections that were instrumented for the measurement of the FRP hoop strains. This, at least partly, explains the lower than expected k_ε values observed in this study. Thus, the strain reduction factors reported in Table 3 are best be treated as lower-bound values to be expected from specimens having similar properties to those reported in this study. The actual ultimate confinement ratios $f_{lu,a}/f'_{co}$ that were calculated using the experimentally recorded hoop rupture strains $\varepsilon_{h,rup}$ are also provided in Table 3 and are used in the calculation of the strength and strain enhancement coefficients k_1 and k_2 as discussed in the following section.

Effect of Loading Pattern

In Table 3, the comparison of the ultimate strengths and strains of companion specimens that were tested either monotonically or cyclically indicates that, in general, both f'_{cc} and ε_{cu} increase with the presence of load cycles. Although this observation is true for both NSC and HSC specimens confined with AFRP or CFRP, results reported in Table 3 indicate that the observed improvement is

more pronounced in AFRP-confined specimens and is particularly notable for N-A-3L and H-A-4L series specimens. Similar improvements were reported previously by two of the few existing studies (i.e., Lam et al. (2006) and Demir et al. (2010)) that looked into the influence of unloading and reloading cycles on the ultimate condition of FRP-confined concrete. On the other hand, the average k_ε values reported in Table 3 suggest that load cycles did not have a pronounced effect on the recorded hoop rupture strains. This observation does not agree well with the one reported herein regarding the influence of load cycles on the ultimate strength and axial strain of FRP-confined concrete. Furthermore, both Lam et al. (2006) and Demir et al. (2010) reported an observed increase in the hoop rupture strains in the presence of unloading/reloading cycles. It is clear that further research is required on the axial cyclic behavior of FRP-confined concrete to better understand the influence of load cycles on the development of FRP hoop strains and on the strain reduction factor k_ε.

Effect of Unconfined Concrete Strength

Comparison of N-A-2L and H-A-6L series specimens in Table 3, which had similar f_{lu} / f'_{co} ratios, indicate that both the ultimate strength and strain enhancement ratios (f'_{cc} / f'_{co} and $\varepsilon_{cu} / \varepsilon_{co}$) are lower for HSC specimens than for NSC specimens under both monotonic and cyclic loading conditions. Another important observation from Table 3 is that k_ε values of HSC specimens are consistently lower than those of NSC specimens. This observation, which is also supported by those from the other recent studies conducted by the first Author's research group at the University of Adelaide (Wang 2009; Li 2011), suggests that strain reduction factor k_ε is concrete strength dependant. Furthermore, although it was not directly stated by the authors of the original studies, a similar trend can be observed from the test results of a few other studies reported in the literature on FRP-confined HSC (Eid et al. 2009; Cui and Sheikh 2010; Xiao 2010). Further research on FRP-confined HSC is required for an in-depth examination of this important observation.

Lower recorded hoop rupture strains can, at least partly, explain the lower strength and strain enhancement ratios (f'_{cc}/f'_{co} and $\varepsilon_{cu}/\varepsilon_{co}$) observed in the HSC specimens of the present study. However, to demonstrate that the performance difference between the NSC and HSC specimens cannot be explained exclusively by the lower hoop rupture strains of the HSC specimens, strength and strain enhancement coefficients (k_1 *and* k_2) were calculated and are presented in Table 3 for each series of specimens. These values were based on the general form of one of the most widely recognized ultimate condition expressions reported in the literature by Lam and Teng (2003):

$$\frac{f'_{cc}}{f'_{co}} = 1 + 3.3\frac{f_{lu,a}}{f'_{co}} \tag{9}$$

$$\frac{\varepsilon_{cu}}{\varepsilon_{co}} = 1.75 + 12\left(\frac{f_{lu,a}}{f'_{co}}\right)\left(\frac{\varepsilon_{h,rup}}{\varepsilon_{co}}\right)^{0.45} \tag{10}$$

Strength and strain enhancement coefficients (k_1 and k_2) given in Table 3 were calculated from the experimental results by replacing the constant values given in Eqs. 9 and 10 of Lam and Teng's model (i.e., 3.3 and 12) with k_1 and k_2, respectively. It can be seen in Table 3 that the average values of both the strength and strain enhancement coefficients are consistently lower for the HSC specimens than the NSC specimens even when reduced k_ε values are applied in calculating the actual confining pressures $f_{lu,a}$ of the HSC specimens. This suggests that direct application of the existing ultimate condition expressions, which were based almost exclusively on test data from FRP-confined NSC, to FRP-confined HSC can lead to significant overestimations of the ultimate conditions. In particular, the strength enhancement of FRP-confined HSC would be largely overestimated by these expressions if they are to be applied to lightly or moderately confined HSC, such as H-C-4L, H-C-6L and H-A-4L series specimens of the present study. As has also recently been stated by Xiao et al (2010), it is clear that much more work is needed to better understand the behavior of FRP-confined HSC.

Effect of FRP Type

Comparison of H-A-4L and H-C-6L series specimens in Table 3, which had similar concrete strengths and confining pressures, indicates a similar level of strength enhancement (f'_{cc}/f'_{co}) for the AFRP- and CFRP-confined specimens. On the other hand, the level of strain enhancement ($\varepsilon_{cu}/\varepsilon_{co}$) observed in the AFRP-confined specimens is significantly higher than that in the CFRP-confined specimens. This was expected, as the dependency of the ultimate strain enhancement ratio to the rupture strain of the confinement material, or rather to the hoop rupture strain, has been documented previously (e.g. Lam and Teng 2003, 2004) and has now been incorporated into some of the more accurate FRP confinement models.

The comparison of the average k_ε values given in Table 3 for the AFRP- and CFRP-confined HSC specimens, suggests that the type of FRP does not have significant influence on k_ε. This observation, however, is not in agreement with the findings of an on-going research by the first author's research group at the University of Adelaide on the behavior of FRP-confined HSC (Li 2011), where higher k_ε values have been observed for AFRP-confined concrete compared to CFRP-confined concrete. Similar observations about the higher k_ε values of AFRP-confined concrete over CFRP-confined concrete have recently been reported by Dai et al. (2011) based on their experimental studies on FRP-confined NSC. Interestingly, however, despite the favorable behavior of the AFRP-confined concrete as demonstrated by the results of the present study, the area remains largely under-investigated, with majority of the existing studies on FRP-confined concrete focusing on the use of CFRP and GFRP as concrete confinement. Thus, further research is required to better understand how the strain reduction factor k_ε is influenced by the type of FRP.

Effect of Amount of Confinement

It is well understood that there is an intimate relationship between the amount of confinement and the ultimate condition of FRP-confined concrete, and that both the strength and strain enhancement ratios (f'_{cc}/f'_{co} and $\varepsilon_{cu}/\varepsilon_{co}$) increase with increasing confinement ratio ($f_{lu,a}/f'_{co}$). However, a closer

inspection of the strength enhancement coefficients (k_1) reported in Table 3 reveals that, for the HSC specimens the relationship between f'_{cc}/f'_{co} and $f_{lu,a}/f'_{co}$ is not a linear one as suggested by Eq.9. That is, for each series of HSC specimens, k_1 increases with increasing confinement thickness. This can be best explained by referring to the trend of the stress-strain relationships of the HSC specimens shown in Figs. 3(i) and 3(j). For example, the overall descending trend of the second branch of H-C-4L series specimens suggest that confinement provided by 4 layers of 0.117 mm CFRP was not sufficient to provide strength enhancement in 152.5 mm 103 MPa concrete cylinders. As can be seen in Figs. 3(k) and 3(l), when the number of CFRP layers were increased to 6, the specimens (H-C-6L series) exhibited a slightly ascending second branch. It is evident from this comparison that strength enhancement is observed only when the concrete is confined by a confinement system providing a higher than a minimum amount of confinement, which can be defined as threshold confinement amount Therefore, it can be said that only the part of confinement that is over this threshold value contributes directly to the strength enhancement of FRP-confined concrete. Recent experimental studies conducted by the first author's research group at the University of Adelaide indicate that this threshold amount is highly sensitive to the concrete strength and can be up to 10 times as high for ultra HSC of around 120 MPa strength as for standard 30 MPa NSC (Wang 2009; Li 2011). As a result, calculation of k_1 values using the form of Eq.9 that gives no consideration to the threshold confinement amount, leads to extremely low k_1 values for lightly confined HSC specimens (such as H-A-4L and H-C-6L series) as shown in Table 3. It is clear from these observations that for better prediction of the ultimate strength of FRP-confined HSC, there is need for a new expression that can accurately predict the threshold ratio as a function of the concrete strength, and another expression that incorporates this ratio for the calculation of the strength enhancement ratios.

Results reported in Table 3 further indicate that, apart from the variations of k_1 values for the HSC specimens discussed above, for a given series of specimens, strength and strain enhancement

coefficients k_1 and k_2 do not vary significantly with the amount of confinement, suggesting an overall agreement with the forms of Eqs. 9 and 10.

COMPARISON WITH EXISTING STRESS-STRAIN MODELS

In this section, the results of the present study are compared with the cyclic axial stress-strain models developed by Shao et al. (2006) and Lam and Teng (2009). The details of these models can be found in the original papers, and hence are not discussed herein. Figure 7 shows the comparisons of the experimental stress-strain curves with the predictions of Shao's and Lam and Teng's models for two NSC specimens N-A-2L-C1 and N-A-3L-C1 and a HSC specimen H-A-6L-C1. In Shao's model, the stress-strain model for monotonic behavior proposed by Samaan et al. (1998) was used to predict the envelope curve and the curve shape parameter (n) of the model was adjusted to attain the best fit with the experimental curves. In Lam and Teng's model, the researchers' monotonic stress-strain model (Lam and Teng 2003) was used for the prediction of the envelope curve. In the present study, although the shape of the envelope curves was determined based on the expressions proposed by the originators of the models, the test results reported in Table 3 were used to determine the ultimate conditions (i.e. f'_{cc} and ε_{cu}), as there were some differences between the experimental values and model predictions.

Figure 7 illustrates that Lam and Teng's model is highly accurate in predicting both the unloading and reloading paths of FRP-confined NSC. In predicting these paths, both the shapes of the unloading and reloading curves and the predicted values of plastic strains play an important role. As evident from both Fig. 5(a) and Figs 7(b) & 7(d), Lam and Teng's model closely predicts the plastic strains of the NSC specimens of the present study, with only a very slight underestimation. Because Shao's model over-predicts the plastic strains, as illustrated in Fig. 6 and discussed in the previous section, model predictions of the unloading and reloading curves deviate from the experimentally recorded ones in the majority of the load cycles, as shown in Figs. 7(a), 7(c) and 7(e). Furthermore, as was also previously noted by Lam et al (2006), the shape of the unloading curves predicted by

Shao's model does not accurately capture the shape of the experimental curves. On the other hand, provided that reloading initiates at a correctly determined plastic strain, both models predict the reloading paths reasonably accurately, with the parabolic portion defined in Lam and Teng's model for the region where reloading path returns to the envelope curve providing more accurate representation of the experimental curves compared to the fully linear reloading curve given by Shao's model. This is evident from the curves of the NSC specimens shown in Figs 7(a) to 7(d).

Application of both models to the HSC specimens, however, lead to large errors in the estimations of the stress-strain curves as illustrated in Figs. 7(e) & 7(f). In the case of Lam and Teng's model, the deviation from the experimental curves is caused largely by the inaccuracies in the calculation of the plastic strains. The plastic strains calculated by Eq.1 from Lam and Teng's model are not in agreement with the experimentally observed values for the HSC specimens of the present study, as illustrated in Figs. 5(b) & 5(c) and discussed previously. It should be noted that, due to the extremely limited nature of the data available in the literature on the axial cyclic behavior of FRP-confined HSC, Eq. 1 in Lam and Teng's model was calibrated for HSC by using only a few unloading/reloading cycles originally reported by Rousakis (2001) for CFRP-confined HSC. Figure 7(f) illustrates that the performance of Lam and Teng's model degrades greatly when the model is applied to FRP-confined HSC. However, the features of the model that works well for NSC appears to also work well for HSC and the unsatisfactory performance appears to be caused largely by significant underestimation of the experimental plastic strains by Eq. 1. For Lam and Teng's model, which closely predicts the response of FRP-confined NSC, to provide similar levels of accuracy for higher strength concretes, Eq. 1 has to be revised using a larger and more reliable test database. Figure 7(e) illustrates that, unlike Lam and Teng's model, Shao's model's performance does not degrade when the model is applied to HSC, but neither does it improve; that is, the aforementioned shortcomings of the model observed for NSC is also present when the model is applied to HSC. Finally, it is worth noting that it was not possible to accurately predict the envelope curves of the

HSC specimens of the present study using one of the many existing design-oriented stress-strain models developed for FRP-confined monotonic axial compression. This suggests that none of the existing stress-strain models proposed for FRP-confined concrete is capable of predicting the stress-strain relationship of FRP-confined HSC accurately.

CONCLUSIONS

This paper has presented the results of an experimental study on the behavior of FRP-confined NSC and HSC under axial compression. Results from monotonic and cyclic compression tests on AFRP and CFRP-confined concrete specimens have been presented and discussed. The test results have also been compared with two cyclic axial stress-strain models for FRP-confined concrete. Based on the results and discussions presented in the paper the following conclusions can be drawn:

1. The envelope stress-strain curve of cyclically loaded FRP-confined concrete closely follows the stress-strain curve of the same concrete under monotonic loading. This is shown to be true for CFRP-confined HSC and AFRP-confined NSC and HSC.
2. The residual plastic strain of FRP-confined concrete is linearly related to the envelope unloading strain, and this relationship does not appear to be influenced significantly by: i) the amount of confinement; ii) the type of FRP; and iii) the unconfined concrete strength.
3. In general, the presence of unloading/reloading cycles leads to an increase in the ultimate strength and strain of FRP-confined concrete.
4. For a given actual confinement ratio $f_{lu,a}/f'_{co}$, both the strength enhancement and strain enhancement ratios decrease with the increase of unconfined concrete strength. Furthermore, the average hoop rupture strain $\varepsilon_{h,rup}$ also decreases with increasing unconfined concrete strength. Therefore, direct application of the existing FRP-confined concrete stress-strain models to FRP-confined HSC can lead to significant overestimation of the ultimate condition of FRP-confined HSC.

5. Concrete experiences a similar level of strength enhancement when confined with AFRP and CFRP jackets that provide the same actual confining pressure $f_{lu,a}$. On the other hand, the ultimate strain of the same concrete increases more significantly through AFRP confinement.

In addition to the general conclusions of the experimental study reported herein, the following observations can be made based on the comparison of the test results of the present study with two cyclic axial stress-strain models for FRP-confined concrete:

- The axial cyclic stress-strain model proposed by Lam and Teng (2009) is highly accurate in predicting both the unloading and reloading paths of FRP-confined NSC. The model closely predicts the shapes of the unloading and reloading curves and accurately estimates the plastic strains. When the model is applied to HSC specimens, on the other hand, the model predictions deviate significantly from the experimental results; this is caused largely by the inaccuracies in the calculation of the plastic strains of FRP-confined HSC.
- Comparisons between the results of the present study and the predictions of the cyclic stress-strain model proposed by Shao et al. (2006) indicated that this model predicts the reloading paths reasonably accurately, but it consistently overestimates the residual plastic strains and does not accurately capture the shape of the unloading paths.

Finally, it is important to note that among over 50 design-oriented monotonic stress-strain models published in the literature none is able to correctly predict the stress-strain behavior of FRP-confined HSC. There is a need for a stress-strain model that can accurately predict the monotonic behavior of FRP-confined HSC, and more work is required to better understand and model the behavior of FRP-confined HSC.

REFERENCES

Abbasnia, R., and Ziaadiny, H. (2010). “Behavior of concrete prisms confined with FRP composites under axial cyclic compression.” *Journal of Engineering Structures*, 32(3), 648-655.

Almusallam, T. H. (2007). “Behaviour of normal and high-strength concrete cylinders confined with E-Glass/Epoxy composite laminates.” *Composites Part B-Engineering*, 38(5-6), 629-639.

Bahn, B. Y., and Hsu, Cheng-Tzu T. (1998). “Stress-strain behavior of concrete under cyclic loading.” *ACI Materials Journal*, 95(2), 178-193.

Berthet, J. F., Ferrier, E., and Hamelin, P. (2005). “Compressive behaviour of concrete externally confined by composite jackets. Part A: Experimental study.” *Construction and Building Materials, Elsevie*r, 19, 223-232.

Binici, B. (2005). “An analytical model for stress-strain behavior of confined concrete.” *J. Eng. Struct.*, 27(7), 1040-51.

Cui, C., and Sheikh, S.A. (2010). “Experimental study of normal- and high-strength concrete confined with fiber-reinforced polymers.” *Journal of Composites for Construction, ASCE,* 14(5), 553-561.

Dai, J. G., Bai, Y. L., and Teng, J. G. (2011). “Behavior and modeling of concrete confined with FRP composites of large deformability.” *Journal of Composites for Construction, ASCE,* 10.1061/(ASCE)CC.1943-5614.0000230

Demir, C., Kolcu, K., and Ilki, A. (2010). “Effects of loading rate and duration on axial behavior of concrete confined by fiber-reinforced polymer sheets” *Journal of Composites for Construction, ASCE*, 14(2), 146-151.

Eid, R., Roy, N., and Paultre, P. (2009). “Normal- and high-strength concrete circular elements wrapped with FRP composites.” *Journal of Composites for Construction, ASCE*, 13(2), 113-124.

Fahmy, M. and Wu, Z. (2010). “Evaluating and proposing models of circular concrete columns confined with different FRP composites” *Composites Part B: Engineering.* 41(3) pp 199-213.

Fam, A. Z., and Rizkalla, S. H. (2001). “Confinement model for axially loaded concrete confined by circular fiber-reinforced polymer tubes.” *ACI Struct. J.*, 98(4), 451-61.

Ilki, A., and Kumbasar, N. (2003). "Compressive behavior of carbon fiber composite jacketed concrete with circular and non-circular cross sections." *Journal of Earthquake Eng.*, 7(3), 381–406.

Jiang, T., and Teng, J. G. (2007). "Analysis-oriented stress-strain models for FRP-confined concrete." *J. Eng. Struct*., 29(11), 2968-2986.

Karsan, I. D., and Jirsa, J. O. (1969). "Behavior of concrete under compressive loadings." *Journal of Structural Division, ASCE*, 95, 2543-2563.

Lam, L., and Teng, J. G. (2003). "Design-oriented stress-strain model for FRP-confined concrete." *Constr. And Building Materials*, 17, 471-489.

Lam, L., and Teng, J. G. (2004). "Ultimate condition of fiber reinforced polymer-confined concrete." *Journal of Composites for Construction, ASCE*, 8(6), 539-548.

Lam, L., Teng, J. G., Cheung, Y., and Xiao, Y. (2006). "FRP-confined concrete under axial cyclic compression." *Cement and Concrete Composites*, 28, 949-958.

Lam, L., and Teng, J. G. (2009). "Stress-strain model for FRP-confined concrete under cyclic axial compression." *Engineering Structures*, 31, 308-321.

Li, D. (2011). "Stress-strain relationship of concrete confined by FRP tubes." Master's Thesis, *The School of Civil, Environmental and Mining Engineering, The University of Adelaide*, Adelaide, Australia.

Mandal, S., Hoskin, A., and Fam, A. (2005). "Influence of concrete strength on confinement effectiveness of fiber-reinforced polymer circular jackets." *ACI Structural Journal*, 102(3), 383-392.

Martinez, S., and Nilson, H. N. and Slate, F. O. (1984). "Spirally reinforced high-strength concrete columns." *ACI Structural Journal*, 81(5), 431-442.

Mirmiran, A., and Shahawy, M. (1997). "Behavior of concrete columns confined by fiber composites." *ASCE J. Struct. Eng.*, 123(5), 583-90.

Ozbakkaloglu, T., and Saatcioglu, M. (2006). “Seismic behavior of high-strength concrete Columns confined by fiber reinforced polymer tubes.” *Journal of Composites for Construction, ASCE*, 10(6), 538-549.

Ozbakkaloglu, T., and Saatcioglu, M. (2007). “Seismic performance of square high-strength concrete columns in FRP stay-in-place formwork.” *Journal of Structural Engineering, ASCE*, 133(1), 44-56.

Ozbakkaloglu, T. and Oehlers, D. J. (2008). “Manufacture and testing of a novel FRP tube confinement system.” *Engineering Structures*, 30, 2448-2459.

Pessiki, S., Harries, K. A., Kestner, J. T., Sause, R. and Ricles, J. M. (2001). “Axial behavior of reinforced concrete columns confined with FRP jackets.” *Journal of Composites for Construction, ASCE*, 5(4), 237-245.

Razvi, S., and Saatcioglu, M. (1994). “Strength and deformability of confined high-strength concrete columns,” *ACI Structural Journal*, 91(6), 678-687.

Rodrigues CC, Silva MG. (2001). “The behavior of GFRP reinforced concrete columns under monotonic and cyclic axial compression.” Composites in constructions, proceedings of the international conference. Lisse, The Netherlands: A.A. Balkema Publishers; p. 245–50.

Rousakis, T.C. (2001). “Experimental investigation of concrete cylinders confined by carbon FRP sheets under monotonic and cyclic axial compression load.” *Research Report 01:2*, Division of Building Technology, Chalmers University of Technology.

Sakai, J., and Kawashima, K. (2006). “Unloading and reloading stress-strain model for confined concrete.” *Journal of Structural Engineering*, ASCE, 132(1), 112-122.

Samaan, M., Mirmiran, A., Shahawy, M. (1998). “Modeling of concrete confined by fiber composites.” *Journal of Str. Eng., ASCE*, 124(9), 1025-31.

Shao, Y., Zhu, Z., and Mirmiran, A. (2006). “Cyclic modeling of FRP-confined concrete with improved ductility.” *Cement and Concrete Composites*, 28, 959-968.

Tasdemir, M. A., Tasdemir, C., Jefferson, A. D., Lydon, F. D., and Barr, B. I. G. (1998). "Evaluation of strains at peak stresses in concrete: a three-phase composite model approach." *Cem. Concr. Res.*, 20(4), 301-18.

Vincent, T., and Ozbakkaloglu, T. (2009). "Influence of concrete strength and fibre type on the compressive behaviour of FRP-confined high-strength concrete." *Proceedings of 9th International Symposium on Fiber Reinforced Polymer Reinforcement for Concrete Structures (FRPRCS-9)*, 13-15 July, Sydney, Australia.

Wang, G. (2009) "Compressive behaviour of concrete confined by aramid FRP tubes", Masters Thesis, *The School of Civil, Environmental and Mining Engineering, The University of Adelaide*, Adelaide, Australia.

Wu, H. L., Wang, Y. F., Yu, L., and Li, X. R. (2009). "Experimental and computational studies on high-strength concrete circular columns confined by aramid fiber-reinforced polymer sheets." *Journal of Composites for Construction, ASCE*, 13(2), 125-134.

Xiao, Q. G., Teng, J. G., and Yu, T. (2010). "Behavior and modeling of confined high-strength concrete." *Journal of Composites for Construction, ASCE*, 14(3), 249-259.

Xiao, Y., and Wu, H. (2000). "Compressive behavior of concrete confined by carbon fiber composite jackets." *J. Mater. Civil Eng.*, 12(2), 139-46.

Yong, Y. Y., Nour, M., and Nawy, E. G. (1988). "Behavior of lateral confined high-strength concrete under axial loads," *Journal of Structural Engineering, ASCE*, 114(2), 332-350.

Table 1. Properties of test specimens

Loading pattern	Confinement Material	Number of FRP Layers	Specimen	f'_{co} (MPa)	ε_{co} (%)
Monotonic	AFRP	2	N-A-2L-M1	39	0.21
			N-A-2L-M2	39	0.21
		3	N-A-3L-M1	39	0.21
			N-A-3L-M2	39	0.21
		4	H-A-4L-M1	100	0.34
			H-A-4L-M2	102	0.34
		6	H-A-6L-M1	106	0.35
			H-A-6L-M2	106	0.35
	CFRP	4	H-C-4L-M1*	100	0.34
			H-C-4L-M2	108	0.35
		6	H-C-6L-M1	110	0.35
			H-C-6L-M2*	94	0.33
Cyclic	AFRP	2	N-A-2L-C1	38	0.21
			N-A-2L-C2	39	0.21
		3	N-A-3L-C1	39	0.21
			N-A-3L-C2	39	0.21
		4	H-A-4L-C1	100	0.34
			H-A-4L-C2	102	0.34
		6	H-A-6L-C1	104	0.34
			H-A-6L-C2	106	0.35
	CFRP	4	H-C-4L-C1	100	0.34
			H-C-4L-C2	100	0.34
		6	H-C-6L-C1	109	0.35
			H-C-6L-C2	105	0.35

*FRP tube-encased

Table 2. Properties of fiber sheets as provided by the manufacturer

Type	Nominal thickness t_f (mm/ply)	Tensile strength f_{fu} (MPa)	Ultimate tensile strain ε_{fu} (%)	Elastic modulus E_f (GPa)	Weight (g/m^2)
Carbon	0.117	3800	1.55	240	200
Aramid	0.200	2900	2.50	120	290

Table 3. Test results of FRP-confined concrete cylinders

Specimen	f'_{cc} (MPa)	ε_{cu} (%)	$\varepsilon_{h,rup}$ (%)	f_{lu}/f'_{co}	fl_{ue}/f'_{co}	f'_{cc}/f'_{co} Average	$\varepsilon_{cu}/\varepsilon_{co}$ Average	k_1 Average	k_2 Average	k_ε Average
N-A-2L-M1	69.2	2.32	1.71	0.40	0.28	1.75	10.9	2.82	13.8	0.68
N-A-2L-M2	67.1	2.30	1.56	0.40	0.25					
N-A-3L-M1	85.0	2.86	1.66	0.61	0.40	2.21	14.1	2.86	11.2	
N-A-3L-M2	87.6	3.11	1.84	0.61	0.45					
H-A-4L-M1	122.3	1.45	1.18*	0.32	0.15	1.19	4.0	1.26	8.4	0.46
H-A-4L-M2	118.7	1.29	1.29	0.31	0.16					
H-A-6L-M1	154.7	1.70	1.10*	0.45	0.20	1.45	4.9	2.33	9.7	
H-A-6L-M2	153.2	1.70	1.07	0.45	0.19					
H-C-4L-M1	98.9	0.93	0.89	0.23	0.13	0.97	2.7	N/A	5.5	0.55
H-C-4L-M2	103.3	0.96	0.81	0.21	0.11					
H-C-6L-M1	122.3	1.13	0.94	0.31	0.19	1.22	3.4	1.17	5.8	
H-C-6L-M2	124.4	1.16	0.78	0.37	0.18					
N-A-2L-C1	64.3	2.25	1.50	0.42	0.25	1.67	10.7	2.67	14.6	0.68
N-A-2L-C2	64.3	2.25	1.56	0.40	0.25					
N-A-3L-C1	97.4	4.04	1.76	0.61	0.43	2.59	20.0	3.46	14.9	
N-A-3L-C2	104.5	4.43	2.02	0.61	0.49					
H-A-4L-C1	136.4	1.82	1.24	0.32	0.16	1.30	5.1	2.00	13.1	0.50
H-A-4L-C2	125.4	1.63	1.10	0.31	0.14					
H-A-6L-C1	157.2	1.87	1.16	0.46	0.21	1.56	5.8	2.39	9.5	
H-A-6L-C2	170.9	2.13	1.45	0.45	0.26					
H-C-4L-C1	102.3	1.07	0.69	0.23	0.10	0.99	3.2	N/A	8.9	0.48
H-C-4L-C2	96.0	1.06	0.81*	0.23	0.12					
H-C-6L-C1	123.7	1.14	0.64	0.31	0.13	1.19	3.3	1.21	7.6	
H-C-6L-C2	129.9	1.16	0.81	0.33	0.17					

* The average hoop rupture strain was calculated from 2 strain gauges.

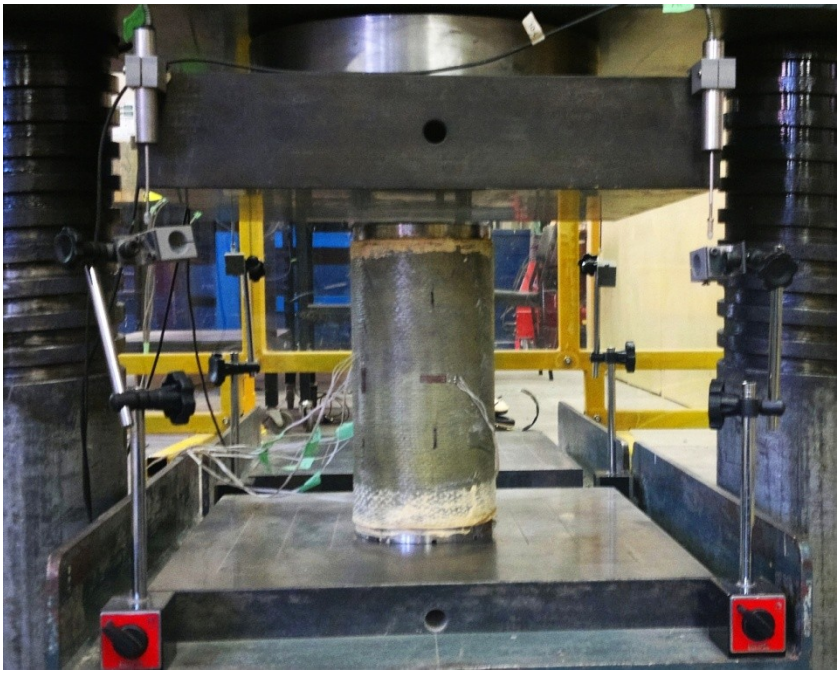

(a)

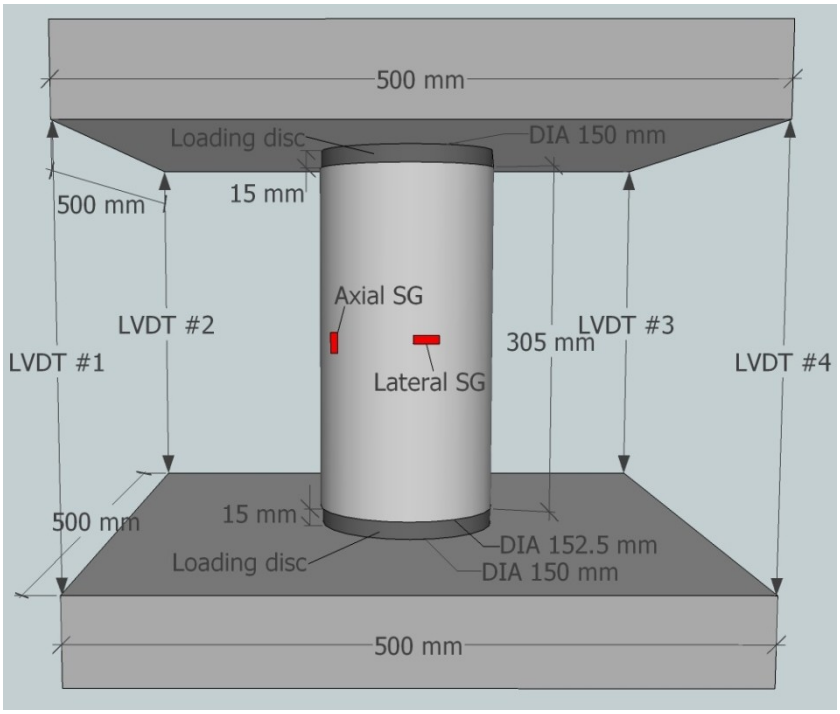

(b)

Figure 1. Test setup used in axial compression tests: (a) Specimen before testing; (b) Technical illustration

(a) (b)

Figure 2. Typical failure modes of test specimens: (a) NSC specimen; (b) HSC specimen

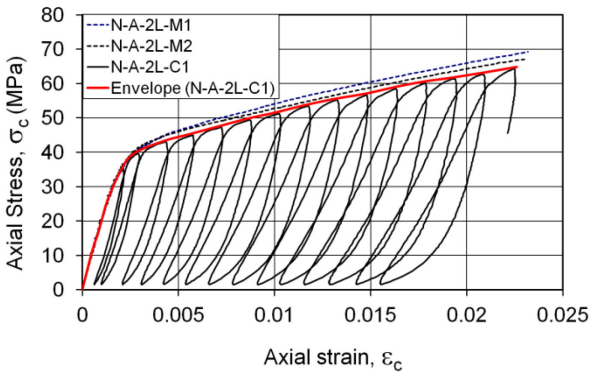
N-A-2L-M1
N-A-2L-M2
N-A-2L-C1
Envelope (N-A-2L-C1)
Axial Stress, σc (MPa)
Axial strain, εc

(a)

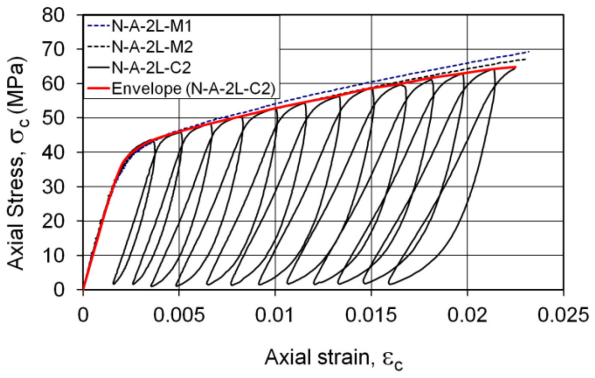
N-A-2L-M1
N-A-2L-M2
N-A-2L-C2
Envelope (N-A-2L-C2)
Axial Stress, σc (MPa)
Axial strain, εc

(b)

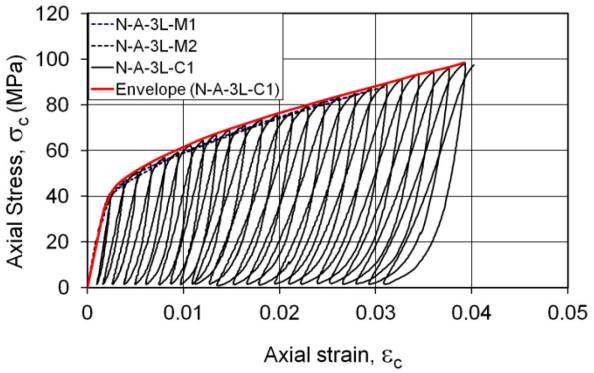
N-A-3L-M1
N-A-3L-M2
N-A-3L-C1
Envelope (N-A-3L-C1)
Axial Stress, σc (MPa)
Axial strain, εc

(c)

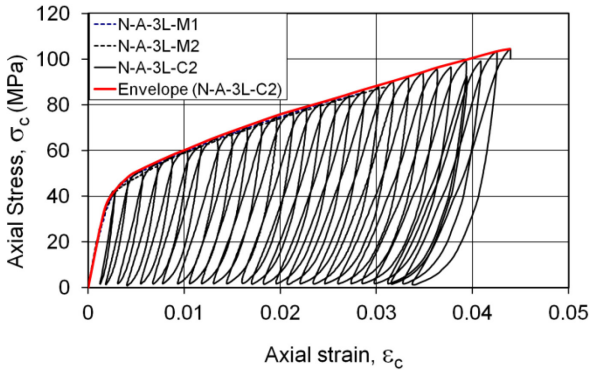
N-A-3L-M1
N-A-3L-M2
N-A-3L-C2
Envelope (N-A-3L-C2)
Axial Stress, σc (MPa)
Axial strain, εc

(d)

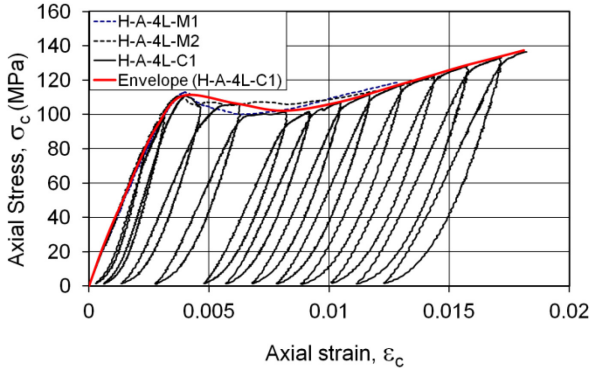
H-A-4L-M1
H-A-4L-M2
H-A-4L-C1
Envelope (H-A-4L-C1)
Axial Stress, σc (MPa)
Axial strain, εc

(e)

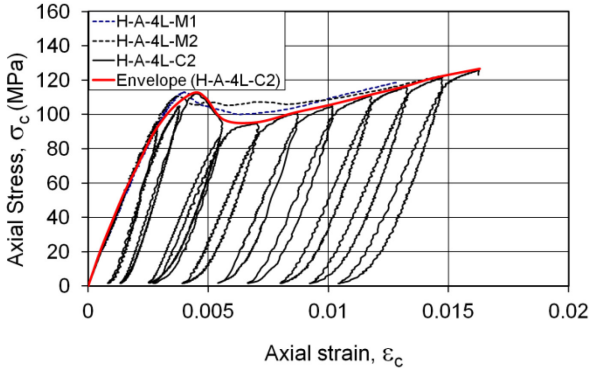
H-A-4L-M1
H-A-4L-M2
H-A-4L-C2
Envelope (H-A-4L-C2)
Axial Stress, σc (MPa)
Axial strain, εc

(f)

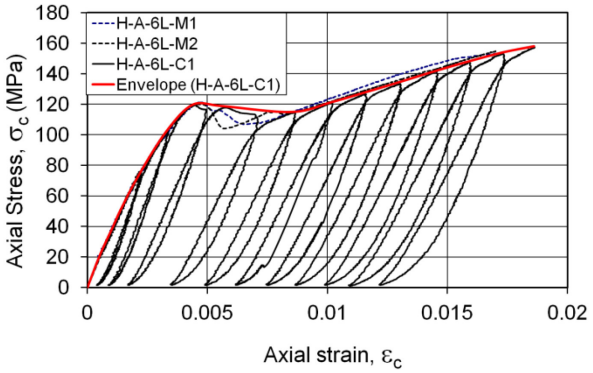
H-A-6L-M1
H-A-6L-M2
H-A-6L-C1
Envelope (H-A-6L-C1)
Axial Stress, σc (MPa)
Axial strain, εc

(g)

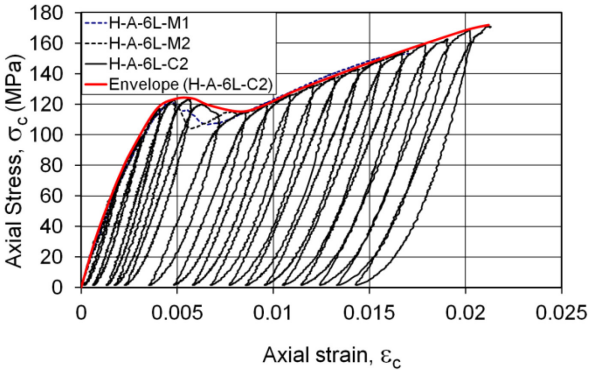
H-A-6L-M1
H-A-6L-M2
H-A-6L-C2
Envelope (H-A-6L-C2)
Axial Stress, σc (MPa)
Axial strain, εc

(h)

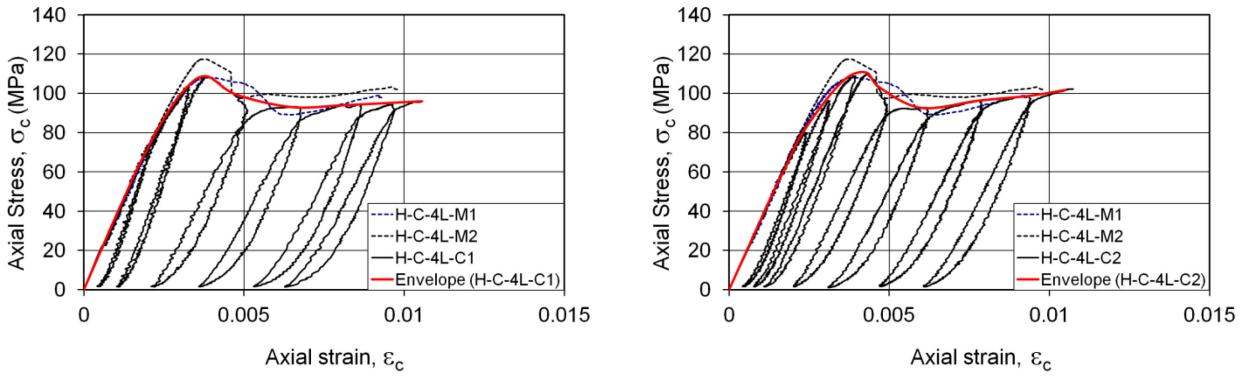

(i)

(j)

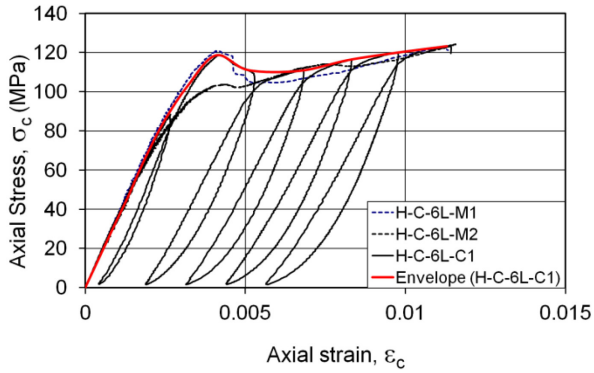

(k)

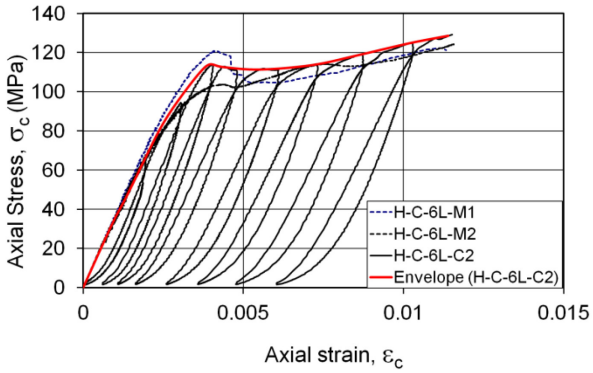

(l)

Figure 3. Axial stress-strain curves of test specimens: (a) N-A-2L Series-1; (b) N-A-2L Series-2; (c) N-A-3L Series-1; (d) N-A-3L Series-2; (e) H-A-4L Series-1; (f) H-A-4L Series-2; (g) H-A-6L Series-1; (h) H-A-6L Series-2; (i) H-C-4L Series-1; (j) H-C-4L Series-2; (k) H-C-6L Series-1; (l) H-C-6L Series-2

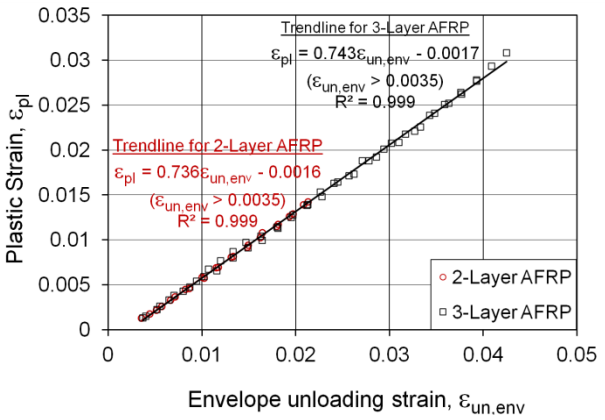

(a)

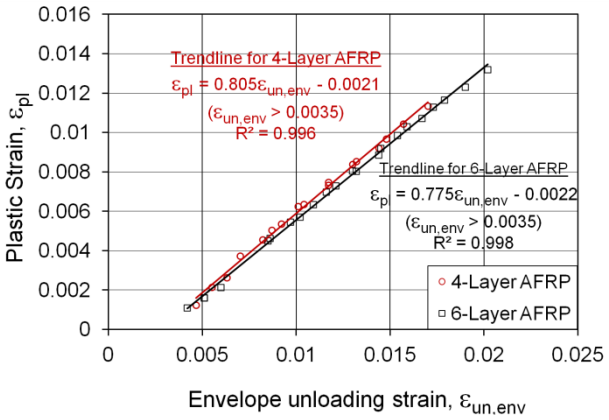

(b)

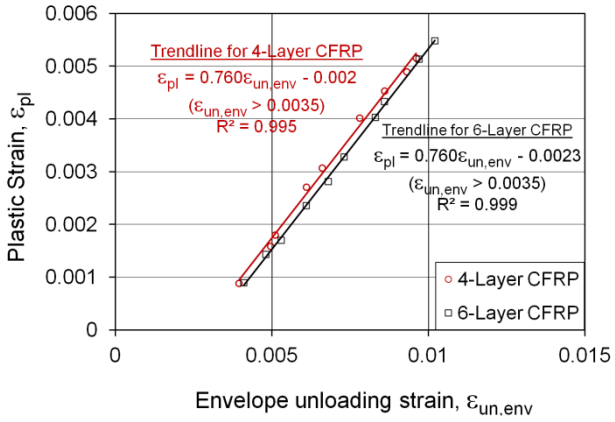

(c)

Figure 4. Plastic strain-envelope unloading strain relationships of test specimens: (a) AFRP-confined NSC; (b) AFRP-confined HSC; (c) CFRP-confined HSC

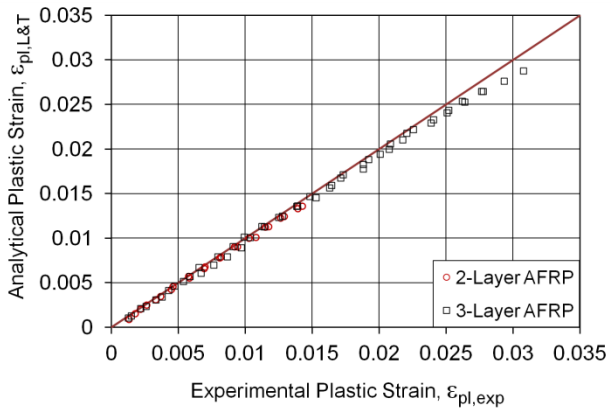

(a)

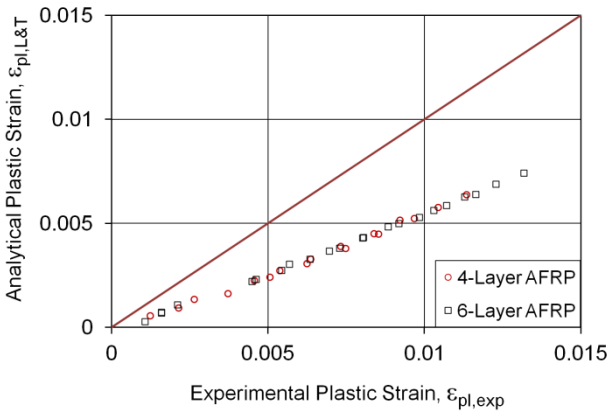

(b)

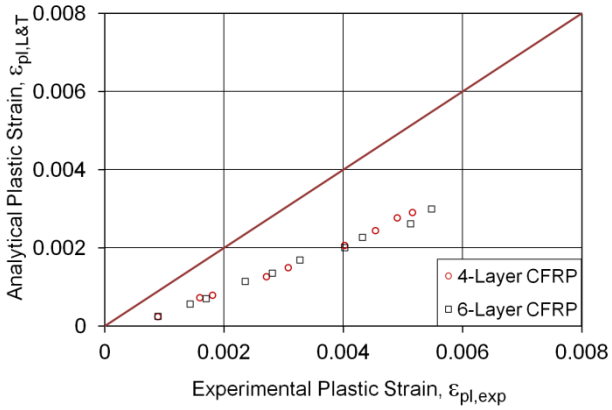

(c)

Figure 5. Comparison of experimentally recorded plastic strains with predictions of Lam and Teng's model: (a) AFRP-confined NSC; (b) AFRP-confined HSC; (c) CFRP-confined HSC

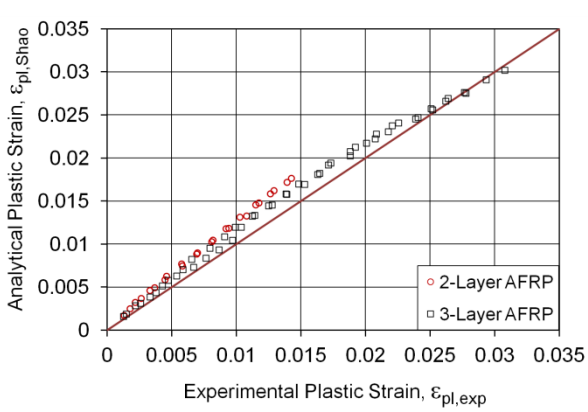

(a)

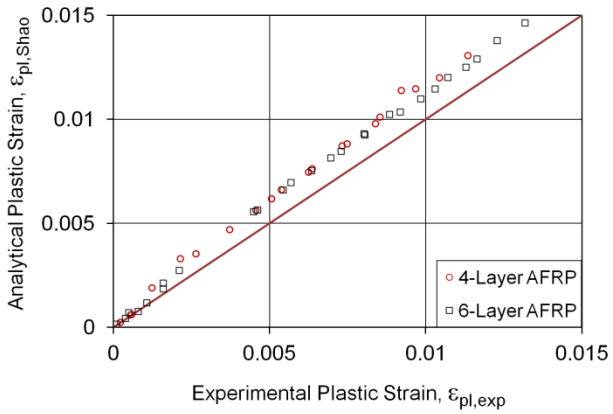

(b)

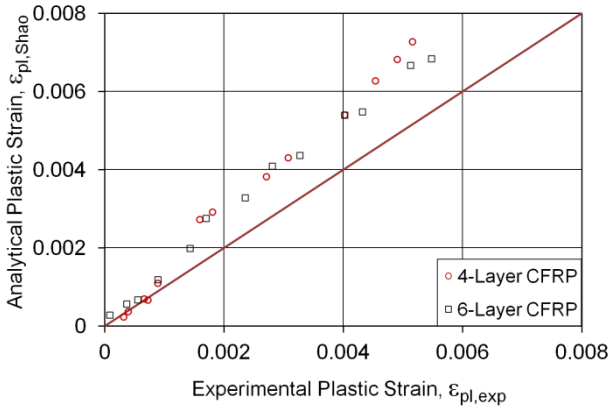

(c)

Figure 6. Comparison of experimentally recorded plastic strains with predictions of Shao's model: (a) AFRP-confined NSC; (b) AFRP-confined HSC; (c) CFRP-confined HSC

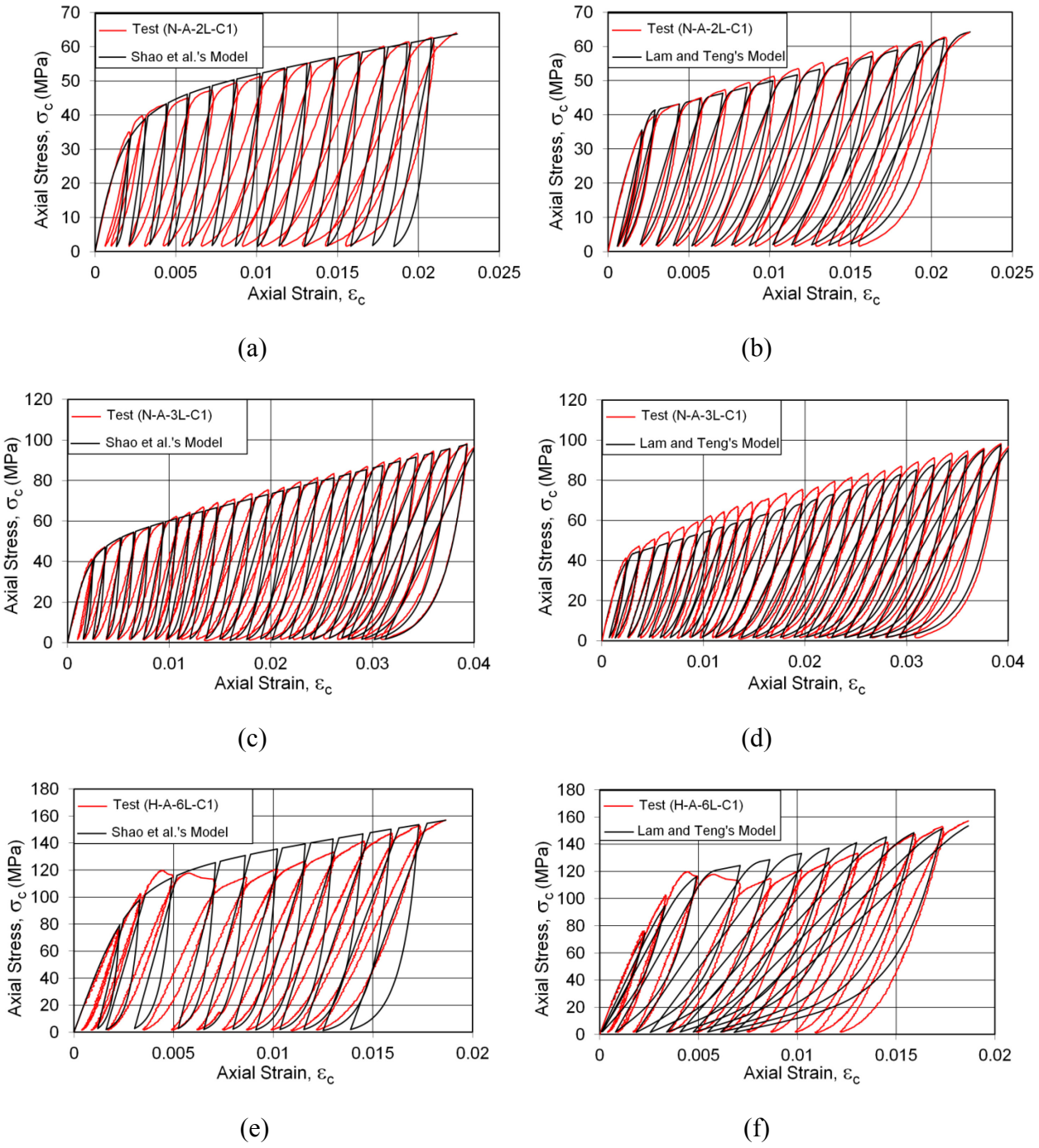

Figure 7. Comparison of experimental cyclic stress-strain curves with predictions of Shao's and Lam & Teng's models: (a) Specimen N-A-2L-C1 vs Shao's model; (b) Specimen N-A-2L-C1 vs Lam & Teng's model; (c) Specimen N-A-3L-C1 vs Shao's model (d) Specimen N-A-3L-C1 vs Lam & Teng's model; (e) Specimen H-A-6L-C1 vs Shao's model (f) Specimen H-A-6L-C1 vs Lam & Teng's model.